

Thermally Induced Anomaly in the Shear Behavior of Magnetite at High Pressure

Yongtao Zou,^{1,2,*} Wei Zhang,³ Ting Chen,² Xing-ao Li,⁴ Chun-Hai Wang,¹ Xintong Qi,² Shanmin Wang,¹ Tony Yu,⁵ Bingbing Liu,⁶ Yanbin Wang,⁵ Robert C. Liebermann,² Yusheng Zhao,¹ and Baosheng Li²

¹*Academy for Advanced Interdisciplinary Studies, and Department of Physics, Southern University of Science and Technology, Shenzhen 518055, China*


²*Mineral Physics Institute, and Department of Geosciences, State University of New York, Stony Brook, N.Y. 11794, United States*

³*School of Science, Southwest University of Science and Technology, Mianyang, Sichuan 610064, China*

⁴*School of Science, Nanjing University of Posts and Telecommunications, Nanjing 210046, China*

⁵*Center for Advanced Radiation Sources, The University of Chicago, Chicago, I.L. 60637, United States*

⁶*State Key Laboratory of Superhard Materials, Jilin University, Changchun 130012, China*

 (Received 23 September 2017; revised manuscript received 04 April 2018; published 9 August 2018)

Thermoelasticity and acoustic velocities of polycrystalline magnetite are studied at simultaneously high pressures and temperatures up to 8.6 GPa and 1123 K using ultrasonic interferometry in conjunction with *in situ* x-ray techniques. Here, we report temperature-driven anomalies in the shear behavior at temperatures up to ~ 450 K, together with pressure-induced softening in the shear properties. Fitting the current data to finite strain equations, we obtain the bulk and shear moduli, as well as their pressure and temperature dependences, namely $B_{S0} = 173.2(5)$ GPa, $G_0 = 55.5(2)$ GPa, $\partial B_S/\partial P = 2.99(9)$, $\partial G/\partial P = -0.23(3)$, $\partial B_S/\partial T = -0.0209(10)$ GPa/K, $\partial G/\partial T = 0.0042(4)$ GPa/K, $(\partial^2 B_S/\partial T^2)_P = -1.7(1) \times 10^{-5}$ GPa²/K², and $(\partial^2 G/\partial T^2)_P = -2.5(1) \times 10^{-5}$ GPa²/K². The origin of the thermally induced anomaly in the shear modulus for Fe₃O₄ magnetite is ascribed to the coupling of local atomic distortions and short-range charge ordering of sixfold-coordinated Fe²⁺ and Fe³⁺ ions at the octahedral sites in the inverse-spinel structure. These findings or results provide high-*P* thermoelasticity data of magnetite and present an opportunity to gain a good understanding of the underlying mechanism of temperature-driven anomalies in magnetite-based solid solutions and spinel-structured materials for their applications in extreme conditions.

DOI: [10.1103/PhysRevApplied.10.024009](https://doi.org/10.1103/PhysRevApplied.10.024009)

I. INTRODUCTION

Magnetite (Fe₃O₄) is of great interest because of the importance of understanding the properties of spinel-structured materials and iron oxides in the Earth's interior, as well as its industrial applications in magnetic and electronic materials, and in nanocomposites for its physical behaviors [1–12]. At ambient conditions, magnetite is half-metallic and has an inverse spinel structure, in which the tetrahedral fourfold-coordinated *A* site is occupied by Fe³⁺, and the octahedral *B* site is occupied by both Fe²⁺ and Fe³⁺. Because the magnetic moments of Fe ions are antiparallel at the tetrahedral and octahedral sites, magnetite exhibits a ferromagnetic state below the Curie temperature of ~ 860 K [13]. At ambient pressure, magnetite undergoes a metal-insulator transition below the Verwey temperature ($T_V \approx 122$ K), where an abrupt

increase of electrical resistivity was observed in association with a cubic-to-monoclinic phase transition [14]. Above the Verwey transition, it is accepted that the magnetite adopts an inverse-spinel structure with Fe³⁺ ions in *A* sites and *B* sites in a mixed-valence Fe^{2.5+} state [15–20]. However, several previous studies indicate the existence of short-range order of polaronic character [15–20], which is correlated with the critical softening of C_{44} elastic constant on cooling [15,16], softening of the surface phonons [17], low-energy fluctuations of the lattice distortions [18], anomalous phonon broadening [19], and the Fermi-surface nesting features [20]. However, to date, the short-range ordering and/or its related abnormal properties above the Verwey transition or at temperatures higher than ~ 122 K is still not well understood.

Recent high-pressure studies on magnetite raise enormous controversies about the interpretation of the electronic and structural behavior at pressures between 6 and 16 GPa [8,9,14,21–25], ranging from the inverse-normal

*zouyt@sustc.edu.cn

spinel transition [14], iron high-spin to intermediate-spin transition [3,21], pressure-tuned ideal inverse-spinel structure [23], and the decreased Fe—O bond length caused by the discontinuous changes in the local oxygen coordinates [24]. Recently, *in situ* magnetoresistivity measurements revealed a magnetoresistivity transition at a pressure of ~ 6.0 GPa owing to the half-metal to metal transition [8], in agreement with the previous electrical resistivity measurement on the metallization of magnetite at room temperature and pressures above 8 GPa [9]. However, the more recent studies on magnetite at high pressure by Lin *et al.* [25] using the combination of inelastic x-ray scattering, x-ray diffraction, and Raman spectroscopy techniques propose that the origin of the abnormal elastic and vibrational behaviors of magnetite at ~ 8 GPa is due to the local site distortions and the charge ordering between Fe^{2+} and Fe^{3+} ions at the octahedral sites in the inverse spinel.

Elastic bulk and shear moduli as well as their pressure and temperature dependences are important parameters in understanding the high P - T behavior and physical properties upon compression. The compressibility and bulk modulus (B) of magnetite have been studied by static compression experiments [21,23,25–31] and first-principle calculations [8,32], however, the reported values are quite scattered with significant discrepancies, ranging from 155 to 215 GPa with the associated pressure derivative (B') in a wide range of 2.9–7.5. Sound velocities of single-crystal magnetite at high pressure were studied by Isida *et al.* [33] up to 1.2 kbar, and the pressure dependences of the elastic constants C_{11} and C_{44} were reported to be anomalous. Recently, elasticity of a natural magnetite was measured at pressures up to 8.7 GPa using gigahertz ultrasonic interferometry in a diamond-anvil cell [34], yielding a pressure-marker-dependent $\partial B_S/\partial P$, namely $\partial B_S/\partial P = 5.1(1)$ for a quartz pressure marker and $\partial B_S/\partial P \approx 3$ for a ruby pressure marker, together with a negative $\partial G/\partial P = -0.1(1)$.

To date, the high-pressure behavior of magnetite is still under debate and studies under high temperature are rather scarce, especially for the shear-related properties. In this study, simultaneous high-pressure and high-temperature sound-velocity measurements on polycrystalline Fe_3O_4 magnetite are conducted in a multianvil apparatus using ultrasonic interferometry in conjunction with x-ray diffraction and radiographic imaging techniques [34–39]. Here, we report the observations of temperature-driven and pressure-induced anomalies in the shear modulus of Fe_3O_4 magnetite, as well as the possible mechanisms underlying these abnormal behaviors. An internally consistent set of thermoelasticity data for magnetite is derived based on the measured velocities and density data by a pressure-standard-free fitting procedure using the third-order finite-strain equations [37].

II. EXPERIMENTAL DETAILS

The polycrystalline Fe_3O_4 magnetite specimen used in the present study was commercially obtained from Trans-Tech. Inc., USA. Compressional (P) and shear (S) wave velocities of polycrystalline Fe_3O_4 magnetite at high pressure and high temperature are measured using ultrasonic interferometry in conjunction with *in situ* x-ray diffraction and x radiography in a multianvil apparatus at GSECARS (Sector 13) of the Advanced Photon Source (APS), Argonne National Laboratory. Details of this experimental setup are described elsewhere [35–39]. Briefly, the pressure-transmitting medium is a MgO octahedron. Graphite is used as a heater. A dual-mode LiNbO_3 transducer ($10^\circ Y$ cut) is mounted with a high-temperature epoxy on a truncated corner of a WC anvil cube, which can generate and receive both P and S signals simultaneously. To minimize the loss of acoustic energy, all surfaces along the acoustic path, including the ends of the WC cube with transducer mounted, alumina buffer rod, and the specimen, are well polished using $1\text{-}\mu\text{m}$ diamond paste. Inside the cell assembly, the front surface of the sample is in contact with an alumina (Al_2O_3) buffer rod via a gold film ($2\ \mu\text{m}$) to improve their mechanical coupling, whereas the rear surface of the sample is backed by NaCl pressure marker. Temperatures are monitored with a $\text{W}_{97}\text{Re}_3\text{-W}_{75}\text{Re}_{25}$ thermocouple. Travel times for P and S waves are simultaneously measured using the transfer function method with standard deviation of ~ 0.4 ns for S waves and ~ 0.2 ns for P waves [35–39]. The sample length at high pressure and high temperature is directly obtained by x-radiographic imaging method; the precision of this direct measurement of sample length is estimated to be 0.2–0.4% [37,38]. During our experiments, x-ray diffraction patterns for both the specimen and pressure marker are collected using a solid-state detector, which is mounted on a stage behind the high-pressure press set at a diffraction angle of $2\theta \approx 6.09^\circ$. The collected x-ray diffraction patterns of the sample are refined to determine the unit-cell volume, from which the densities at high pressures and temperatures are obtained, as shown in Table I.

III. RESULTS AND DISCUSSION

At ambient conditions, the polycrystalline Fe_3O_4 magnetite specimen has an inverse-spinel structure (space group $Fd\bar{3}m$, no. 227), and the crystal structure is shown in Fig. 1(a). Prior to our ultrasonic measurement experiments, the purchased polycrystalline magnetite specimen is characterized by x-ray diffraction and SEM observations, showing that the starting magnetite is a pure cubic spinel structure and free of visible microcracks. SEM images of from the current ultrasonic measurements show that the recovered specimen exhibits an equilibrated

TABLE I. Physical properties of Fe₃O₄ magnetite derived from the current ultrasonic measurements in conjunction with synchrotron x-ray diffraction at simultaneously high pressures and temperatures.

P^a (GPa)	T (K)	ρ (g/cm ³)	L (mm)	V_P (km/s)	V_S (km/s)	B_S (GPa)	G (GPa)	ν	E (GPa)
8.59	1123	5.293(1)	0.662	6.773	3.061	176.7	49.6	0.372	136.0
7.35	1123	5.254(2)	0.662	6.759	3.077	173.7	49.7	0.369	136.2
8.04	923	5.315(1)	0.661	6.867	3.137	180.9	52.3	0.368	143.1
7.04	923	5.284(1)	0.662	6.843	3.145	177.7	52.3	0.366	142.8
5.90	923	5.249(1)	0.665	6.824	3.161	174.6	52.4	0.363	143.0
7.96	673	5.355(1)	0.660	6.970	3.169	188.5	53.8	0.370	147.3
6.84	673	5.323(1)	0.660	6.948	3.177	185.4	53.7	0.368	146.9
5.90	673	5.295(1)	0.662	6.914	3.191	181.3	53.9	0.365	147.1
4.35	673	5.248(1)	0.665	6.902	3.217	177.6	54.3	0.361	147.9
7.82	473	5.379(1)	0.659	7.015	3.176	192.4	54.3	0.371	148.8
6.57	473	5.344(1)	0.660	7.000	3.184	189.6	54.2	0.370	148.4
5.64	473	5.317(2)	0.662	6.980	3.203	186.3	54.6	0.367	149.1
4.12	473	5.273(2)	0.665	6.968	3.230	182.6	55.0	0.363	150.0
7.35	300	5.386(2)	0.660	7.045	3.163	195.5	53.9	0.374	148.1
6.31	300	5.357(1)	0.660	7.015	3.172	191.8	53.9	0.371	147.9
5.07	300	5.322(2)	0.662	6.995	3.191	188.2	54.2	0.369	148.3
4.12	300	5.295(1)	0.665	6.982	3.219	185.0	54.9	0.365	149.8

^aThe pressures are calculated using the equation $P = -3K_{S(0,T)}\varepsilon(1 - 2\varepsilon)^{2.5}[1 + 3(4 - K'_{S(0,T)})\varepsilon/2]$. The uncertainties are less than 0.3% in elastic wave velocities and $\sim 1.5\%$ in the derived elastic moduli.

and homogeneous microstructure without significant grain growth after annealing at the highest P - T conditions of 8.6 GPa and 1123 K, as shown in Fig. 1(b). After annealing and resintering at ~ 8.6 GPa and 1123 K, the bulk density of the recovered magnetite specimen from this study by the Archimedes immersion method is $\sim 5.18(2)$ g/cm³, reaching $\sim 99.5\%$ of the theoretical density of 5.21 g/cm³. This means that the porosity of the specimen is about 0.5%, resulting in a negligible effect on the elasticity of polycrystalline magnetite within uncertainties [35–39]. SEM energy-dispersive x ray measurements on the recovered specimen yield a slightly nonstoichiometric composition of Fe_{2.98(1)}O₄, which is exactly the same value with the starting counterpart within uncertainties. A typical x-ray diffraction pattern of magnetite at the peak P - T conditions of 8.6 GPa and 1123 K is shown in Fig. 1(c), indicating that the specimen is still a spinel-structured material, and no other phases such as wüstite or hematite are observed.

The schematic experimental setup and P - T path for the present ultrasonic measurements in conjunction with synchrotron x-ray study are shown in Figs. 2(a) and 2(b), respectively. In this experiment, we perform four heating-cooling cycles at pressures up to ~ 8.6 GPa and temperatures up to 1123 K. The sample is annealed at a peak temperature of each cycle for several minutes to release nonhydrostatic stress accumulated during cold compression and decompression. All the ultrasonic and x-ray diffraction measurements are conducted upon cooling after annealing at high pressures. Representative acoustic signals observed at the peak P - T conditions of ~ 8.6 GPa and 1123 K are shown in Fig. 1(d). It is found that

echoes from the interfaces of anvil-buffer rod, buffer-rod sample, and sample pressure marker can be clearly identified, ensuring a precise determination of the compressional and shear travel times even at the highest P - T conditions.

Comparison of x-ray diffraction patterns of magnetite at various pressures and temperatures is shown in Fig. 3(a), indicating that no structural phase transitions/transformations occur in magnetite during the current measurements up to ~ 8.6 GPa and 1123 K. On the basis of the travel time and sample length data in Table II, the compressional (V_P) and shear (V_S) velocities of Fe₃O₄ magnetite are derived. As shown in Fig. 3(b), while V_P increases monotonically with pressures, however, V_S exhibits an anomalous negative pressure dependence. By fitting the present acoustic velocity data to the third-order finite strain equations [35–38], we obtain $V_P = 6.90(2)$ km/s and $V_S = 3.28(2)$ km/s at ambient conditions. Our current data are $\sim 4\%$ lower than those derived from single-crystal measurements on natural magnetite [$V_P = 7.16(3)$ km/s; $V_S = 3.41(2)$ km/s] by Reichmann *et al.* [34]. As clearly seen in Fig. 3(b), our negative pressure-dependence of shear velocity [$\partial V_S/\partial P \approx -0.017(3)$ km s⁻¹/GPa] is almost the same as the negative values for the natural magnetite [34], and for NiFe₂O₄ spinel [40]. By contrast, the pressure dependence of V_P from this study, $\partial V_P/\partial P \approx 0.019(2)$ km s⁻¹/GPa, is significantly smaller than $\partial V_P/\partial P \approx 0.047(1)$ km s⁻¹/GPa for the natural magnetite [34], and $\partial V_P/\partial P \approx 0.044(1)$ km s⁻¹/GPa for NiFe₂O₄ spinel [40], respectively.

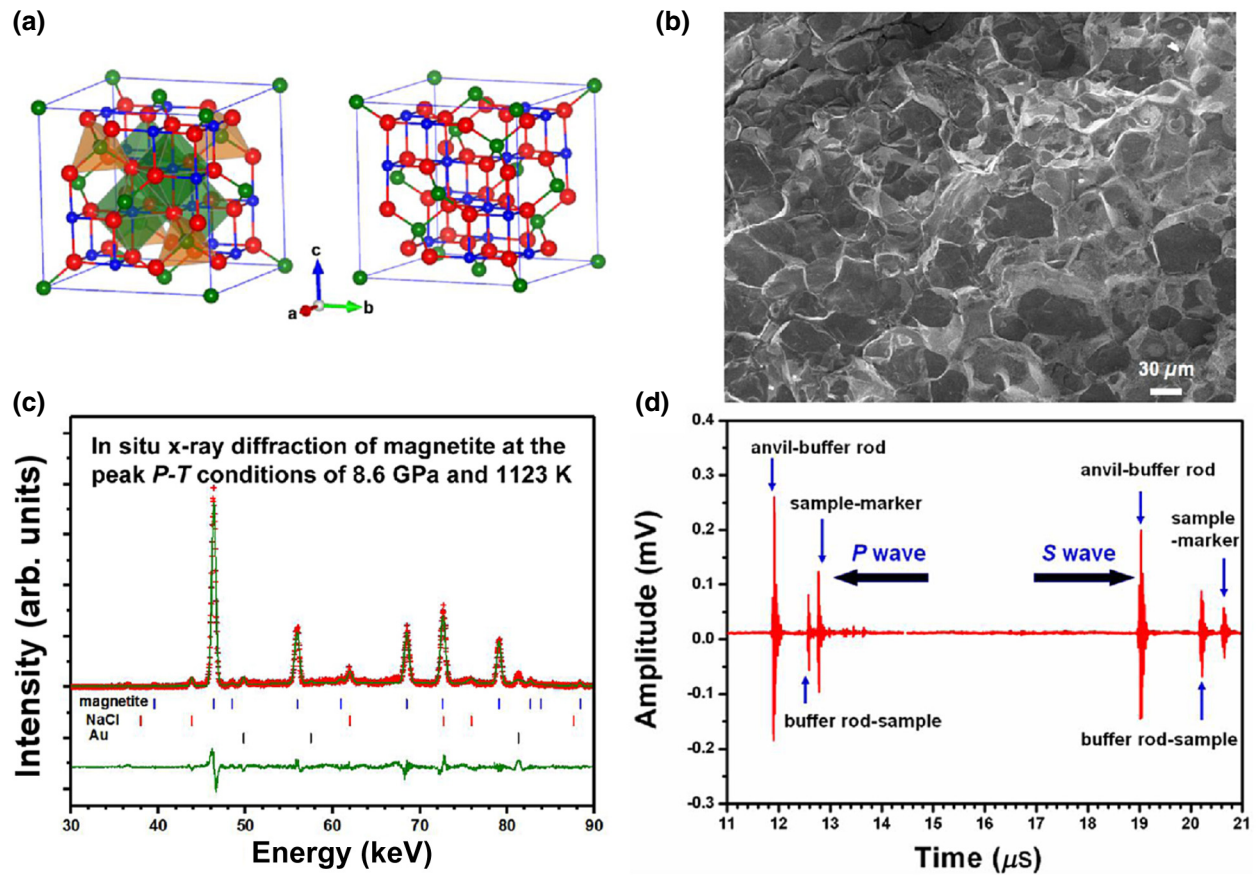


FIG. 1. (a) Crystal structure of Fe_3O_4 magnetite at ambient conditions with a cubic inverse-spinel structure (space group $Fd\bar{3}m$, no. 227). Large Fe^{3+} ions at tetrahedral sites are represented by green spheres. Red and small blue spheres are oxygen ions and Fe cations (including Fe^{2+} and Fe^{3+}) at the octahedral sites, respectively. (b) SEM image showing the microstructure of the recovered polycrystalline Fe_3O_4 magnetite after the current acoustic velocity measurements. The specimen was free of visible microcracks with an average grain size of about 20–30 μm , exhibiting an equilibrated and homogeneous microstructure. (c) Typical x-ray diffraction pattern of magnetite at the highest P - T conditions of 8.6 GPa and 1123 K, suggesting that the specimen is still a cubic spinel structure without the occurrence of other phases such as wüstite and hematite. The solid green line and red cross represent the Rietveld refinement results (PDF: 76-1849, cubic, $Fd\bar{3}m$ (227)) and observed data, respectively, and the solid green curve at the bottom presents the residuals. The vertical bars are the peak positions of the phases present. The peaks of Au and NaCl are from the gold foil and pressure marker used in this study. (d) Waveform data for P - and S -wave signals of magnetite at the peak P - T conditions of 8.6 GPa and 1123 K.

As shown in Fig. 3(c), our obtained bulk moduli are consistent with those from the recent inelastic x-ray scattering measurements on a stoichiometric single-crystal Fe_3O_4 magnetite by Lin *et al.* [25] within ~ 6.2 GPa, but lower than those from the gigahertz ultrasonic interferometry in a diamond-anvil cell on natural magnetite by Reichmann *et al.* [34]. By contrast, however, our derived shear moduli are in general agreement with those from previous studies using different specimens and techniques [7,34], and no visible discontinuity is observed at pressures up to ~ 7.4 GPa in Fig. 3(c). To examine more closely the structural stability of magnetite upon compression, electrical resistance measurements are conducted at pressures up to ~ 12.8 GPa in a multianvil apparatus [see Fig. 4(a)]. It is found that the resistance decreases continuously with increasing pressures, indicating that the magnetite

specimen becomes a better metallic conductor at higher pressures. This result agrees well with the previous studies on the electrical resistivity of magnetite at high pressure [9,21,25].

Figure 5(a) shows the compressional and shear wave velocities of Fe_3O_4 magnetite along different isotherms under high pressure. The compressional wave velocity exhibits a systematic increase with pressure and decreases with temperature, whereas the shear wave velocity (V_S) shows a negative trend as a function of pressure along all the isothermal temperatures ranging from 300 to 1123 K. The current negative pressure dependence in V_S [$\partial V_S/\partial P = -0.017(3)$ $\text{km s}^{-1}/\text{GPa}$] is in great contrast to previous reports for other spinel-structured materials, such as MgAl_2O_4 [$\partial V_S/\partial P = 0.0022(5)$ $\text{km s}^{-1}/\text{GPa}$] (Ref. [38]) and Mg_2SiO_4 [$\partial V_S/\partial P = 0.021$ $\text{km s}^{-1}/\text{GPa}$] (Ref. [41]).

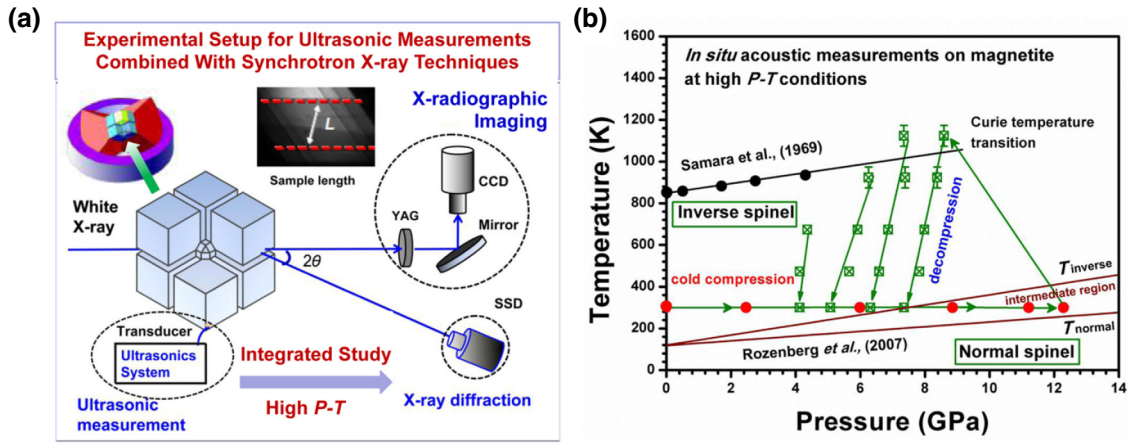


FIG. 2. (a) The experimental setup for the present ultrasonic measurements combined with synchrotron x-ray diffraction. (b) Experimental P - T conditions for the combination of *in situ* x-ray diffraction and ultrasonic measurements on polycrystalline Fe_3O_4 magnetite, as well as the phase diagram of Fe_3O_4 at high pressure and high temperature based on the previous studies [13,14]. The red circle symbols represent the P - T data points upon cold compression, whereas the crossed-green-square symbols are those at high P - T conditions during cooling. The black solid line and circles are the phase boundary for paramagnetic-to-ferrimagnetic transition (Curie temperature) determined by Samara *et al.* [13]. The coordination crossover transition boundaries for the inverse-normal conversion are shown in red lines proposed by Rozenberg *et al.* [14], and the in-between area of these two lines represents the intermediate region of the inverse-normal transition.

As suggested for natural magnetite, the negative pressure dependence originates from the softening shear constant C_{44} under pressures [34]. A closer examination of Fig. 5(a) indicates that, in addition to the negative pressure dependence in V_S , the shear-wave velocities appear to exhibit a positive temperature dependence within 300 and 673 K [see Fig. 5(a)] and then change to a negative dependence above 673 K. This abnormal behavior as a function of temperature has never been observed in magnetite before.

The bulk and shear moduli are calculated using $\rho V_p^2 = B_S + 4G/3$ and $G = \rho V_S^2$, respectively, based on acoustic velocities and densities (Table I), and the results

are shown in Fig. 5(b). Clearly, the thermally induced anomaly in V_S is also observed in the derived shear moduli. We fit all the data collected in the entire P - T conditions of this study to the third-order finite-strain equations to obtain adiabatic ambient-condition bulk and shear moduli as well as their pressure and temperature derivatives and dependences. The detailed data-processing procedure can be found elsewhere [35–38]. With the thermal expansivity $\alpha = 1.425 \times 10^{-5} + 3.65 \times 10^{-8}T$ (Ref. [42]) and Grüneisen parameter $\gamma = 1.33$ from Ref. [33], we obtained the elastic bulk and shear moduli, as well as their pressure and temperature dependences, namely

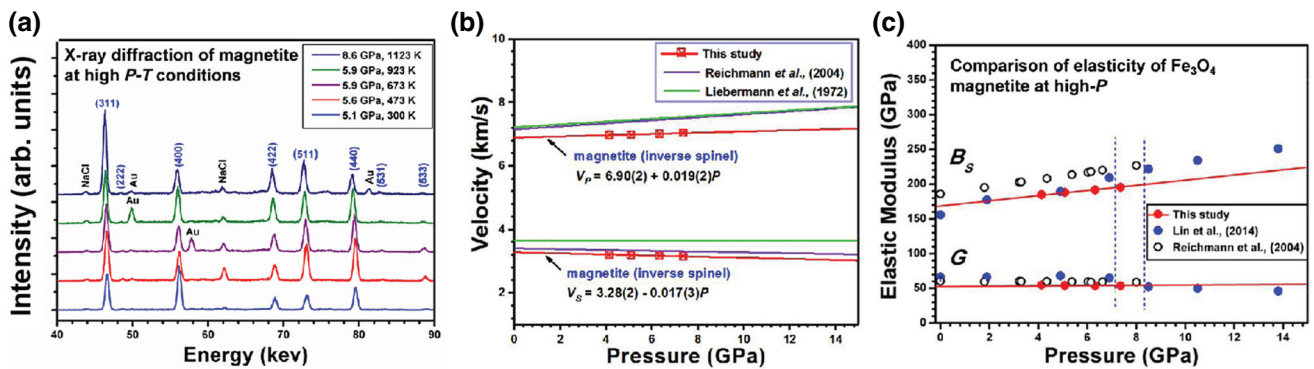


FIG. 3. (a) Selected x-ray diffraction patterns for Fe_3O_4 magnetite at high pressure and high temperature. The peaks of magnetite are indexed (PDF 76-1849), and the peaks labeled by Au and NaCl are from the gold foil and pressure marker used in this study. (b) Compressional (V_p) and shear (V_S) wave velocities for Fe_3O_4 magnetite spinel at high pressure and room temperature (after annealing), in comparison with those from the previous studies. The third-order finite strain fits are shown as red solid lines. (c) Elasticity of bulk and shear moduli of polycrystalline Fe_3O_4 magnetite at high pressure and room temperature, as compared with those from the previous studies by Lin *et al.* [25] (blue symbols) and Reichmann *et al.* [34] (open black symbols), respectively. Red lines are the finite strain fits for this study. Blue vertical lines indicate the transition pressure range around ~ 8 GPa as suggested by Lin *et al.* [25].

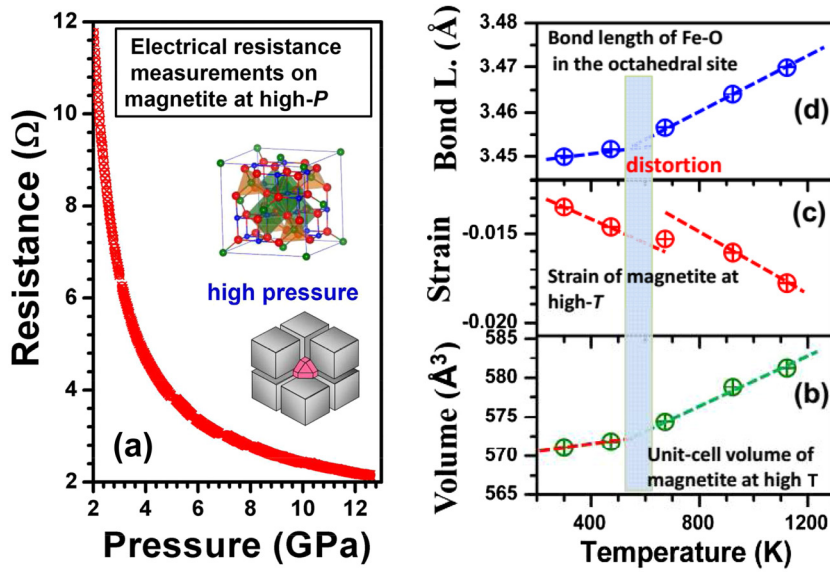


FIG. 4. (a) Electrical resistance measurements of polycrystalline Fe_3O_4 magnetite at high pressure in a multi-anvil apparatus, showing a continuous decrease in electrical resistance with increasing pressures. (b) Unit-cell volume. (c) Strain expressed as $\varepsilon = [1 - (V_{(0T)}/V^{2/3})]/2$. (d) Average Fe—O bond length at the octahedral sites for magnetite against temperature at constant pressure.

$B_{S0}=173.2(5)$ GPa, $G_0 = 55.5(2)$ GPa, $\partial B_S/\partial P = 2.99(9)$, $\partial G/\partial P = -0.23(3)$, $\partial B_S/\partial T = -0.0209(10)$ GPa/K, $\partial G/\partial T = 0.0042(4)$ GPa/K, $(\partial^2 B_S/\partial T^2)_P = -1.7(1) \times 10^{-5}$ GPa²/K², and $(\partial^2 G/\partial T^2)_P = -2.5(1) \times 10^{-5}$ GPa²/K² (see Table II). We note, for most minerals and materials, the cross derivatives of $(\partial^2 B_S/\partial P \partial T)_P$ and $(\partial^2 G/\partial P \partial T)_P$ are in the order of 10^{-4} (Refs. [37,38]), resulting in an overall effect on the pressure derivatives with an order of ~ 0.1 , which is negligible and thus assumed to be zero in this study.

The elasticity of Fe_3O_4 magnetite is summarized in Table II for comparison with those from previous studies on magnetite, wüstite, and other spinel-structured materials [8,26,31,34,38,40–44]. The bulk modulus [$B_{S0}=173.2(5)$ GPa] of Fe_3O_4 magnetite from this study is

generally consistent with the previous experimental data [183(10) and 215(25) GPa from Refs. [26] and [31]] and theoretical results of 182(9) GPa [8] within the mutual uncertainties, but is $\sim 7\%$ lower than that for natural magnetite [34] as well as that by theoretical calculations [43]. As shown in Table II, the pressure derivative of $\partial B_S/\partial P = 2.99(9)$ from this study is in excellent agreement with the recent theoretical result [$B' = 2.90(1)$] [8]. On the other hand, our obtained shear modulus of $G_0 = 55.5(2)$ GPa is significantly lower than that for natural magnetite [34], but larger than the theoretical result of 49.5 GPa [43]. These discrepancies may result from the different pressure ranges and hydrostatic conditions in different experimental studies as well as the well-known trade-off between the bulk modulus and its pressure derivative in equation-of-state fit.

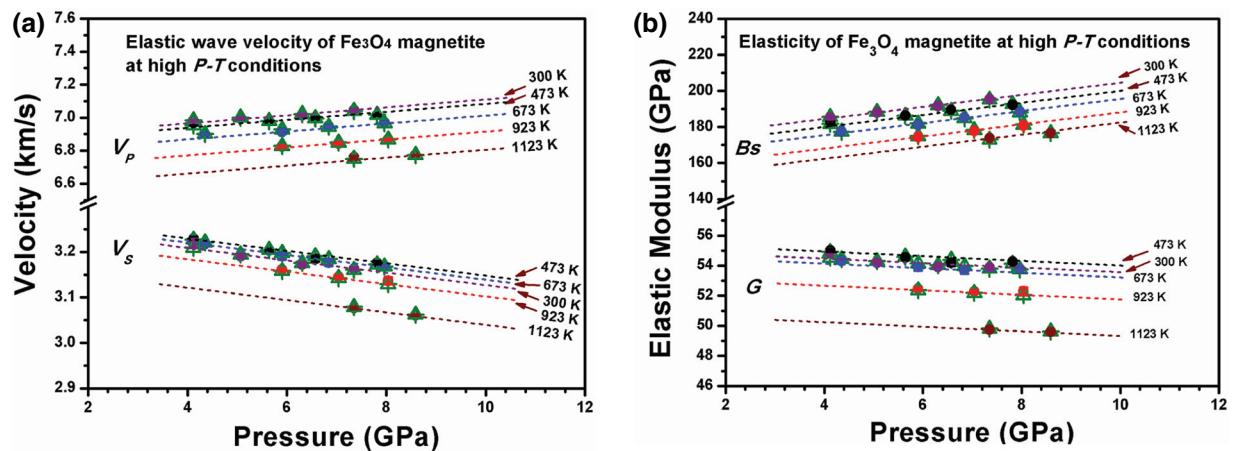


FIG. 5. (a) Finite strain fitting (open triangles) and observed (solid circles) results of compressional (V_p) and shear (V_s) wave velocities of Fe_3O_4 magnetite as a function of pressure and temperature. (b) Finite strain fitting (open triangles) and observed (solid circles) results of elastic bulk (B_s) and shear (G) moduli of Fe_3O_4 magnetite against pressure and temperature. Error bars indicate two standard deviations. Color lines are eye guides for isotherms.

TABLE II. Summary of the elasticity of magnetite, compared with those for other Fe-, Al-, and Si-bearing spinels.

Mater.	B_{S0} (GPa)	G_0 (GPa)	$(\partial B_S/\partial P)_T$	$(\partial G/\partial P)_T$	$(\partial B_S/\partial T)_P$ (GPa/K)	$(\partial G/\partial T)_P$ (GPa/K)	$(\partial^2 B_S/\partial T^2)_P$ (GPa ² /K ²)	$(\partial^2 G/\partial T^2)_P$ (GPa ² /K ²)	Ref.
Fe ₃ O ₄ magnetite	173.2(5)	55.5(2)	2.99(9)	-0.23(3)	-0.0209(10)	0.0042(4)	-1.7(1)×10 ⁻⁵	-2.5(1)×10 ⁻⁵	This study
Fe ₃ O ₄	182(9)	—	2.90(1)	—	—	—	—	—	Ju <i>et al.</i> ^a
Fe ₃ O ₄	183(10)	—	4.0(4)	—	—	—	—	—	Mao <i>et al.</i> ^b
Fe ₃ O ₄	215(25)	—	7.5(40)	—	—	—	—	—	Gerward <i>et al.</i> ^b
Fe ₃ O ₄	187.4	49.5	—	—	—	—	—	—	Roldan <i>et al.</i> ^c
Natural magnetite	186(3)	60 (3)	5.1(1)	-0.1(1)	—	—	—	—	Reichmann <i>et al.</i> ^d
Fe ₂ TiO ₄	121	22.6	—	—	—	0.086	—	-2.344×10 ⁻⁴	Syono <i>et al.</i> ^e
NiFe ₂ O ₄	182.3	71.3	4.41	0.38	-0.019	-0.007	—	—	Liebermann ^f
MgFe ₂ O ₄	176.3(7)	80.1(2)	—	—	-0.032(3)	-0.0012(1)	—	—	Antao <i>et al.</i> ^f
MgAl ₂ O ₄	196.0(9)	109.0(4)	4.60(9)	0.58(3)	-0.022(3)	-0.014(1)	—	—	Zou <i>et al.</i> ^f
Mg ₂ SiO ₄	185(2)	120(1)	4.5(2)	1.5(1)	—	—	—	—	Li ^f

^aFirst-principle calculations (Ref. [8]);

^bStatic compression experiments (DAC, isothermal results) (Refs. [26,31]);

^cFirst-principle calculations (Ref. [43]);

^dGigahertz ultrasonic interferometry (DAC) (Ref. [34]);

^eUltrasonic pulse echo method (Ref. [44]);

^fUltrasonic interferometry (multianvil apparatus) (Refs. [38,40,41,45]);

As clearly seen in Table II, the unusual negative pressure dependence of shear modulus [$\partial G/\partial P = -0.23(3)$] for Fe₃O₄ magnetite from this study is generally consistent with $\partial G/\partial P = -0.1(1)$ for natural magnetite [34] within the mutual uncertainties, but is significantly lower than the weak positive values for nonsilicate spinels (*e.g.* $\partial G/\partial P = 0.58$ for MgAl₂O₄ spinel [38] and $\partial G/\partial P = 0.38$ for NiFe₂O₄ trevovite [40]), as well as the large positive $\partial G/\partial P = 1.5$ for Mg₂SiO₄ silicate spinel [45]. Likely, the origins for the pressure-induced abnormal shear behavior in spinel-structured Fe₃O₄ magnetite ($G' = -0.23$) include both the FeO₆ octahedral distortion upon compression as proposed by Zou *et al.* [38] for nonsilicate spinels, and the magnetoelastic coupling as well as the first-order phase transition to an orthorhombic structure at high pressure by Reichmann *et al.* [34].

To gain insight into mechanism for the thermally induced anomaly in the shear properties, the shear modulus for Fe₃O₄ magnetite as a function of temperature at constant pressure is calculated based on our newly derived thermoelasticity data [Fig. 6(a)], which are compared with those for iron-bearing compounds such as Fe_{0.943}O wüstite and Fe₂TiO₄ ulvöspinel, as well as other spinel-structured materials [see Figs. 6(b) and 6(c)]. As shown in Fig. 6(a), the shear modulus for Fe₃O₄ magnetite increases with temperatures and reaches a maximum value of ~ 55.8 GPa at the temperature of ~ 450 K, above which it decreases with increasing temperature. As shown in Fig. 6(c), this anomalous behavior is quite similar to those of Fe_{0.943}O wüstite and Fe₂TiO₄ ulvöspinel, but is significantly different from the trends for Al- and Fe-bearing spinels such as NiFe₂O₄, MgFe₂O₄ and

MgAl₂O₄, where the shear moduli decrease gradually with temperatures.

To seek a possible structure-related mechanism for the thermally induced anomaly in the shear modulus, the crystal structure of Fe₃O₄ magnetite [Fig. 7(a)] is compared with those of FeO wüstite [Fig. 7(b)] and Fe₂TiO₄ ulvöspinel [Fig. 7(c)]. For cubic wüstite, the anomalous positive $\partial G/\partial T$ in terms of $G = [2C_{44} + (C_{11} - C_{12})]/4$ was proposed to be related to the positive $\partial C_{44}/\partial T$ resulting from the lowering C_{44} near its Néel temperature ($T_N \approx 195$ K). As clearly seen in Fig. 7(a), this unusual behavior in G for wüstite resulted from the lowering C_{44} can persist up to ~ 550 K, the reason for which is proposed to be due to the magnetoelastic interactions and relaxation from exchange coupling between the neighbor Fe²⁺ ions at the octahedral sites, as suggested by Jackson *et al.* [46] and Isaak *et al.* [47]. By contrast, the shear modulus of the inverse-spinel structured Fe²⁺(Fe²⁺Ti⁴⁺)O₄ ulvöspinel increased anomalously with temperatures up to ~ 225 K, which is ~ 83 K higher than its Curie temperature of $T_C \approx 142$ K [44]. As seen from the crystal structure of Fe₂TiO₄ ulvöspinel in Fig. 7(c), there is an absence of Fe³⁺ ions at the octahedral sites. Thus, the origin of the anomalous shear stiffening with temperatures below ~ 225 K in Fe₂TiO₄ ulvöspinel was proposed to be related to the presence of Jahn-Teller Fe²⁺ ions at the tetrahedral sites yielding large magnetostriction, rather than the hopping of electrons and charges between Fe²⁺ and Fe³⁺ at the octahedral sites which may be observed in Fe₂TiO₄-Fe₃O₄ solid solutions by Ishikawa and Syono [44].

For magnetite, the tetrahedral four-coordinated *A* site is occupied by Fe³⁺ ions, and the octahedral *B* site is

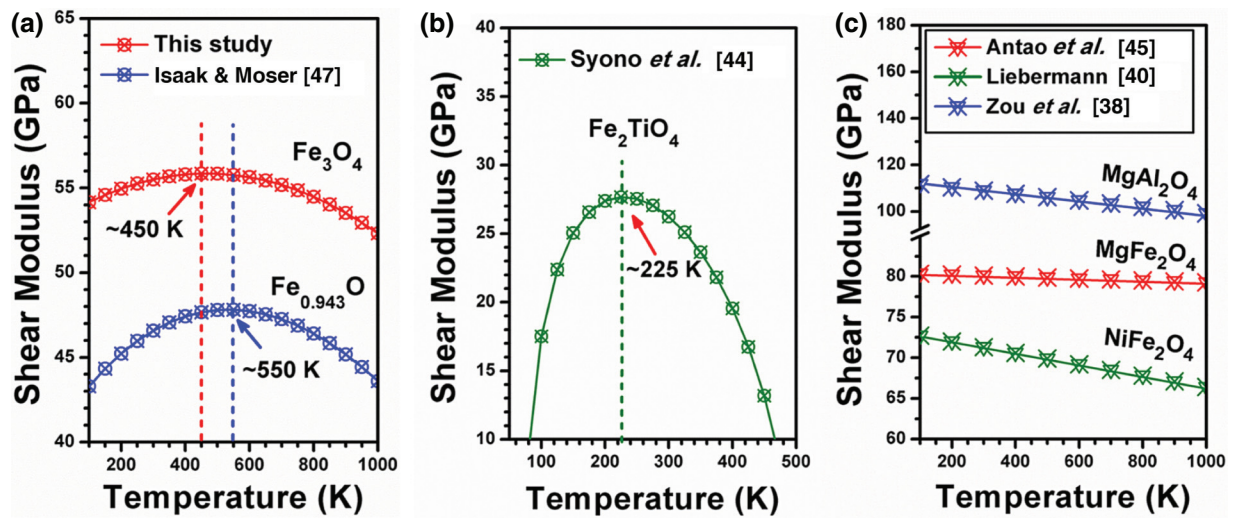


FIG. 6. (a) Anomalous temperature dependence of shear modulus in spinel-structured Fe_3O_4 magnetite at ambient pressure, in comparison with those for $\text{Fe}_{0.943}\text{O}$ wüstite, (b) Fe_2TiO_4 ulvöspinel and (c) other spinel-structured materials such as MgAl_2O_4 , MgFe_2O_4 and NiFe_2O_4 .

occupied by both Fe^{2+} and Fe^{3+} cations at ambient conditions. According to earlier x-ray diffraction structural studies on single-crystal magnetite, $\text{Fe}^{3+}\text{-Fe}^{2+}\text{-Fe}^{3+}$ ions at the octahedral site may form linear three-Fe-site units (called trimerons) with the three-site distortions, which become charge ordered below the Verwey temperature of $T_V \approx 122$ K [4,25]. Above the Verwey transition, it is suggested that magnetite adopts the inverse-spinel structure with Fe^{3+} ions in A sites and B sites in a mixed-valence $\text{Fe}^{2.5+}$ state [15–20]. With increasing temperatures up to ~ 450 K, we postulate that the $\text{Fe}^{3+}\text{-Fe}^{2+}\text{-Fe}^{3+}$ ions, or formed trimerons, may facilitate atomic displacements and distortions, and activate the hopping of electrons or short-range charge ordering between Fe^{2+} and Fe^{3+} at the octahedral sites, resulting in a less symmetrical yet “ideal” inverse spinel structure with a small distortion. The presence of this short-range effect in magnetite above the Verwey temperature is further supported by several previous studies on the existence of short-range interactions of polaronic character in magnetite [15–20], which could be related to a pronounced shear mode stiffening in C_{44}

elastic constant [15,16], softening of the surface phonons [17], low-energy fluctuations of the lattice distortions [18], anomalous phonon broadening [19] and nesting features of the Fermi surface [20].

On the other hand, because of the absence of Fe^{2+} ions at the tetrahedral sites of magnetite, the mechanism for the abnormal shear stiffening below ~ 450 K in magnetite cannot be due to the Jahn-Teller effects as in Fe_2TiO_4 ulvöspinel [44], or the magnetoelastic interactions between the nearest and next-nearest Fe^{2+} ions as proposed in FeO wüstite [46,47]. Moreover, on the basis of the inverse-to-normal spinel model [21,25], the inverse-to-normal phase transition in magnetite is associated with significant changes in the unit-cell volume and local-site symmetry, as well as electrical transport properties. Thus, we rule out the possibility of the inverse-to-normal spinel transition as the mechanism for the anomalous shear stiffening with temperatures of $300\sim 450$ K in magnetite. The unit-cell volume, strain, and average $\text{Fe}\text{—O}$ bond lengths at the octahedral sites for magnetite against temperatures at constant pressure are shown in Figs. 4(b)–(d), indicating that

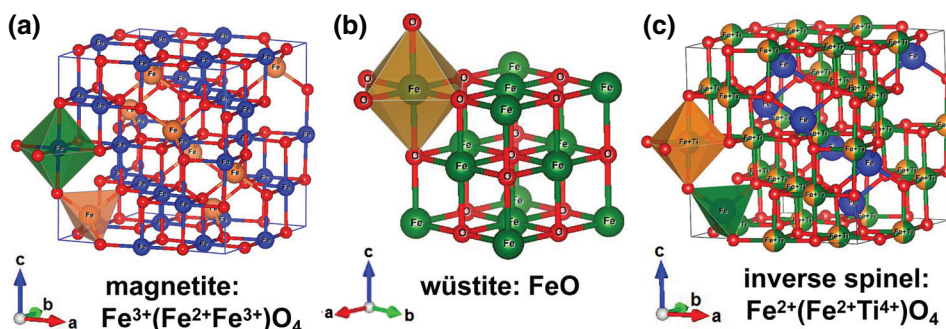


FIG. 7. (a) Crystal structure of inverse spinel-structured Fe_3O_4 magnetite at ambient conditions, in comparison with those of FeO (b) wüstite and Fe_2TiO_4 ulvöspinel (c).

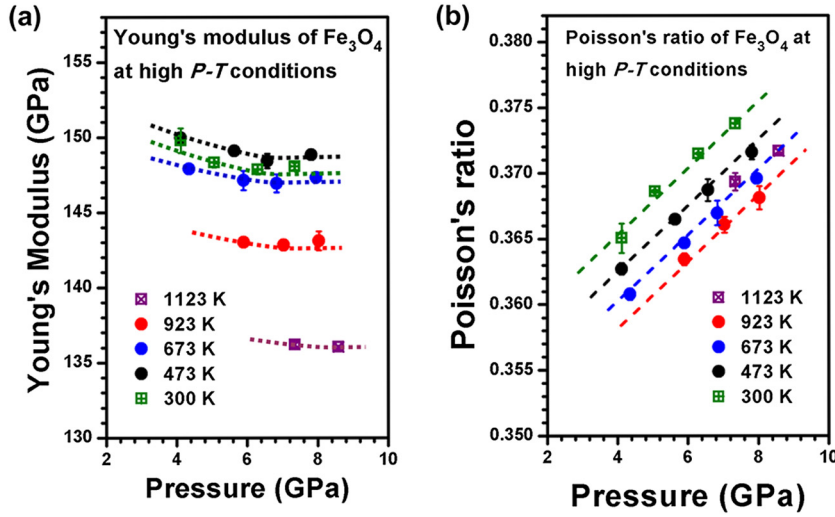


FIG. 8. (a) Young's modulus (E) and (b) Poisson's ratio (ν) of Fe_3O_4 magnetite against pressure and temperature, which is derived by applying $E = 9BG/(3B + G)$ and $\nu = (3B - 2G)/(6B + 2G)$, respectively. The Young's modulus (E) is a measure of the stiffness of a solid material, and Poisson's ratio (ν) provides the fundamental metric by which to compare the performance of materials when strained elastically, in comparing a material's resistance to distortion under mechanical load rather than to altering in volume. Colored lines representing isotherms are a guide for the eye.

the local atomic distortions in FeO_6 octahedra may be another reason for the temperature-driven anomaly, which is supported by the previous neutron scattering measurements on magnetite where low-energy fluctuations of the lattice distortions are observed [18]. Therefore, in addition to the short-range charge ordering of Fe^{2+} and Fe^{3+} ions at the octahedral sites of magnetite, the local atomic distortions should also be responsible for the thermally induced anomaly in the shear modulus above the Verwey temperature. The coupling between local charge ordering and lattice distortions leads ultimately to the structural phase transition with more complicated charge distributions.

It is worth noting that the discovery of the temperature-driven anomaly in the shear properties of Fe_3O_4 magnetite could be also observed in magnetite-based solid solutions or spinel-structured materials with the composition of $M_{3-x}N_x\text{O}_4 = [M_{1-x}^{3+}N_x^{2+}]_{\text{tet}}[M_{1+x}^{3+}M_{1-x}^{2+}]_{\text{oct}}\text{O}_4$ ($M = \text{Fe, Co, Ni}$; $N = \text{Zn}^{2+}, \text{Mg}^{2+}, \dots$). Similarly to magnetite, the mechanism for the predicted temperature-induced anomalies in $[M_{1-x}^{3+}N_x^{2+}]_{\text{tet}}[M_{1+x}^{3+}M_{1-x}^{2+}]_{\text{oct}}\text{O}_4$ spinels above Verwey transition temperatures would be mainly related to the short-range charge ordering of sixfold-coordinated M^{2+} and M^{3+} at the octahedral sites.

IV. CONCLUSIONS

In summary, acoustic velocities and elasticity of Fe_3O_4 magnetite are measured at simultaneously high pressure and high temperature using ultrasonic interferometry in conjunction with synchrotron x-ray diffraction and radiographic imaging techniques. In addition to the pressure-induced softening, we discover a thermally driven anomaly in the shear modulus of magnetite. Using finite strain approaches, the elastic bulk and shear moduli as well as their pressure and temperature dependences are derived from the directly measured

velocities and densities, yielding $B_{S0} = 173.2(5)$ GPa, $G_0 = 55.5(2)$ GPa, $\partial B_S/\partial P = 2.99(9)$, $\partial G/\partial P = -0.23(3)$, $\partial B_S/\partial T = -0.0209(10)$ GPa/K, $\partial G/\partial T = 0.0042(4)$ GPa/K, $(\partial^2 B_S/\partial T^2)_P = -1.7(1) \times 10^{-5}$ GPa²/K², and $(\partial^2 G/\partial T^2)_P = -2.5(1) \times 10^{-5}$ GPa²/K². The anomalous behavior is characterized by the positive temperature dependence and negative pressure derivative for the shear modulus. On the basis of previous studies [36,44,46,47], we propose that the thermally induced anomaly in the shear modulus for Fe_3O_4 magnetite is a manifestation of local atomic distortions and the short-range charge ordering of sixfold-coordinated Fe^{2+} - Fe^{3+} ions at the octahedral sites in the inverse-spinel structure. These results provide high- P thermoelasticity data for magnetite and present an opportunity for better understanding of the underlying mechanism for temperature-driven anomalies in magnetite-based solid solutions and spinel-structured materials and their applications in extreme environments.

ACKNOWLEDGMENTS

We thank Professor David Welch, Professor Songlin Xu, and Professor Ying Li for their discussion in improving the manuscript. This work is supported by the Peacock Team Project of Shenzhen (No. KQTD2016053019134356), Guangdong Innovative & Entrepreneurial Research Team Program (No. 2016ZT06C279), NSF (EAR1045630) and DOE/NNSA (DENA0001815). The current ultrasonic measurement experiments were performed at GeoSoilEnviroCARS (Sector 13), Advanced Photon Source (APS), Argonne National Laboratory, which is supported by the National Science Foundation-Earth Sciences (EAR-1128799) and Department of Energy-GeoSciences (DE-FG02-94ER14466). This research used resources of the Advanced Photon Source, a U.S. Department of Energy (DOE) Office of Science User Facility operated for the

DOE Office of Science by Argonne National Laboratory under Contract No. DE-AC02-06CH11357.

- [1] P. Piekarz, K. Parlinski, and A. M. Oleś, Mechanism of the Verwey transition in magnetite, *Phys. Rev. Lett.* **97**, 156402 (2006).
- [2] J. E. Lorenzo, C. Mazzoli, N. Jaouen, C. Detlefs, D. Mannix, S. Grenier, Y. Joly, and C. Marin, Charge and orbital correlations at and above the Verwey phase transition in magnetite, *Phys. Rev. Lett.* **101**, 226401 (2008).
- [3] Y. Ding, D. Haskel, S. G. Ovchinnikov, Y.-C. Tseng, Y. S. Orlov, J. C. Lang, and H. K. Mao, Novel pressure-induced magnetic transition in magnetite (Fe_3O_4), *Phys. Rev. Lett.* **100**, 045508 (2008).
- [4] M. S. Senn, J. P. Wright, and J. P. Attfield, Charge order and three-site distortions in the Verwey structure of magnetite, *Nature* **481**, 173 (2012).
- [5] Z. Švindrych, Z. Janů, A. Kozłowski, and J. M. Honig, Low-temperature magnetic anomaly in magnetite, *Phys. Rev. B* **86**, 214406 (2012).
- [6] D. Levy, R. Giustetto, and A. Hoser, Structure of magnetite (Fe_3O_4) above the Curie temperature: a cation ordering study, *Phys. Chem. Miner.* **39**, 169 (2012).
- [7] S. Ju, T.-Y. Cai, H.-S. Lu, and C.-D. Gong, Pressure-induced crystal structure and spin-state transitions in magnetite (Fe_3O_4), *J. Am. Chem. Soc.* **134**, 13780 (2012).
- [8] N. Su, Y. Han, Y. Ma, H. Liu, B. Ma, and C. Gao, Pressure-induced magnetoresistivity reversal in magnetite, *Appl. Phys. Lett.* **99**, 211902 (2011).
- [9] S. Todo, N. Takeshita, T. Kanehara, T. Mori, and N. Môri, Metallization of magnetite (Fe_3O_4) under high pressure, *J. Appl. Phys.* **89**, 7347 (2001).
- [10] Z. Zhang and S. Satpathy, Electron states, magnetism, and the Verwey transition in magnetite, *Phys. Rev. B* **44**, 13319 (1991).
- [11] P. Seneor, A. Fert, J.-L. Maurice, F. Montaigne, F. Petroff, and A. Vaurès, Large magnetoresistance in tunnel junctions with an iron oxide electrode, *Appl. Phys. Lett.* **74**, 4017 (1999).
- [12] G. Hu and Y. Suzuki, Negative spin polarization of Fe_3O_4 in magnetite/manganite-based junctions, *Phys. Rev. Lett.* **89**, 276601 (2002).
- [13] G. A. Samara and A. A. Giardini, Effect of pressure on the Néel temperature of magnetite, *Phys. Rev.* **186**, 577 (1969).
- [14] G. K. Rozenberg, Y. Amiel, W. M. Xu, M. P. Pasternak, R. Jeanloz, M. Hanfland, and R. D. Taylor, Structural characterization of temperature- and pressure induced inverse-normal spinel transformation in magnetite, *Phys. Rev. B* **75**, 020102(R) (2007).
- [15] T. J. Moran and B. Lüthi, Elastic and magnetoelastic effects in magnetite, *Phys. Rev.* **187**, 710 (1969).
- [16] H. Schwenk, S. Bareiter, C. Hinkel, B. Lüthi, Z. Kąkol, A. Kozłowski, and J. M. Honig, Charge ordering and elastic Constants in $\text{Fe}_{3-x}\text{Zn}_x\text{O}_4$, *Eur. Phys. J. B* **13**, 491 (2000).
- [17] M. M. Seikh, C. Narayana, P. A. Metcalf, J. M. Honig, and A. K. Sood, Brillouin scattering studies in Fe_3O_4 across the Verwey transition, *Phys. Rev. B* **71**, 174106 (2005).
- [18] (a). S. M. Shapiro, M. Iizumi, G. Shirane, Neutron scattering study of the diffuse critical scattering associated with the Verwey transition in magnetite (Fe_3O_4), *Phys. Rev. B* **14**, 200 (1976); (b). Y. Yamada, N. Wakabayashi, and R. M. Nicklow, Neutron diffuse scattering in magnetite due to molecular polarons, *Phys. Rev. B* **21**, 4642 (1980).
- [19] M. Hoesch, P. Piekarz, A. Bosak, M. Le Tacon, M. Krisch, A. Kozłowski, A. M. Oleś, and K. Parlinski, Anharmonicity due to electron-phonon coupling in magnetite, *Phys. Rev. Lett.* **110**, 207204 (2013).
- [20] A. Bosak, D. Chernyshov, M. Hoesch, P. Piekarz, M. Le Tacon, M. Krisch, A. Kozłowski, A. M. Oleś, and K. Parlinski, Short-Range Correlations in Magnetite above the Verwey Temperature, *Phys. Rev. X* **4**, 011040 (2014).
- [21] S. V. Ovsyannikov, V. V. Shchennikov, S. Todo, and Y. Uwatoko, A new crossover in Fe_3O_4 magnetite under pressure near 6 GPa: modification to ‘ideal’ inverse cubic spinel?, *J Phys. Condens. Matter.* **20**, 172201 (2008).
- [22] F. Baudalet, S. Pascarelli, O. Mathon, J. P. Itie, A. Polian, and J. C. Chervin, Absence of abrupt pressure-induced magnetic transitions in magnetite, *Phys. Rev. B* **82**, 140412(R) (2010).
- [23] Y. W. Fei, D. J. Frost, H. K. Mao, C. T. Prewitt, and D. Häusermann, *In situ* structure determination of the high-pressure phase of Fe_3O_4 , *Am. Miner.* **84**, 203 (1999).
- [24] H. Kobayashi, I. Isogai, T. Kamimura, N. Hamada, H. Onodera, S. Todo, and N. Môri, Structural properties of magnetite under high pressure studied by Mössbauer spectroscopy, *Phys. Rev. B* **73**, 104110 (2006).
- [25] J. F. Lin, J. Wu, J. Zhu, Z. Mao, A. H. Said, B. M. Leu, J. Cheng, Y. Uwatoko, C. Jin, and J. Zhou, Abnormal elastic and vibrational behaviors of magnetite at high pressures, *Sci. Rep.* **4**, 06282 (2014).
- [26] H. -K. Mao, T. Takahashi, W. A. Bassett, G. L. Kinsland, and L. Merrill, Isothermal compression of magnetite to 320 kbar and pressure-induced phase transformation, *J. Geophys. Res.* **79**, 1165 (1974).
- [27] M. P. Pasternak, S. Nasu, K. Wada, and S. Endo, High-pressure phase of magnetite, *Phys. Rev. B* **50**, 6446 (1994).
- [28] L. S. Dubrovinsky, N. A. Dubrovinskaia, C. McCammon, G. K. Rozenberg, R. Ahuja, J. M. Osorio-Guillen, V. Dmitriev, H.-P. Weber, T. Le Bihan, and B. Johansson, The structure of the metallic high-pressure Fe_3O_4 polymorph: Experimental and theoretical study, *J. Phys.: Condens. Matter* **15**, 7697 (2003).
- [29] P. Lazor, O. N. Shebanova, and H. Annersten, High-pressure study of stability of magnetite by thermodynamic analysis and synchrotron x-ray diffraction, *J. Geophys. Res.* **109**, B05201 (2004).
- [30] C. Haavik, S. Stølen, H. Fjellvåg, M. Hanfland, M. Hanfland, and D. Häusermann, Equation of state of magnetite and its high-pressure modification: Thermodynamics of the Fe-O system at high pressure, *Am. Miner.* **85**, 514 (2000).

- [31] L. Gerward and J. S. Olsen, High-pressure studies of magnetite and magnesioferrite using synchrotron radiation, *Appl. Radiat. Isot.* **46**, 553 (1995).
- [32] O. N. Shebanova and P. Lazor, Vibrational modeling of the thermodynamic properties of magnetite (Fe_3O_4) at high pressure from Raman spectroscopic study, *J. Chem. Phys.* **119**, 6100 (2003).
- [33] S. Isida, M. Suzuki, S. Todo, N. Mori, and K. Siratori, Pressure effect on the elastic constants of magnetite, *Phys. B* **219-220**, 638 (1996).
- [34] H. J. Reichmann and S. D. Jackbson, High-pressure elasticity of a natural magnetite crystal, *Am. Miner.* **89**, 1061 (2004).
- [35] W. Liu and B. Li, Elasticity of amorphous zirconium tungstate at high pressure, *Appl. Phys. Lett.* **93**, 191904 (2008).
- [36] W. Liu, B. Li, L. Wang, J. Zhang, and Y. Zhao, Elasticity of ω -phase zirconium, *Phys. Rev. B* **76**, 144107 (2007).
- [37] Y. Zou, T. Irifune, S. Gréaux, M. Whitaker, T. Shinmei, H. Ohfuji, R. Negishi, and Y. Higo, Elasticity and sound velocities of polycrystalline $\text{Mg}_3\text{Al}_2(\text{SiO}_4)_3$ garnet up to 20 GPa and 1700 K, *J. Appl. Phys.* **112**, 14910 (2012).
- [38] Y. Zou, S. Gréaux, T. Irifune, B. Li, and Y. Higo, Unusual pressure effect on the shear modulus in MgAl_2O_4 spinel, *J. Phys. Chem. C* **117**, 24518 (2013).
- [39] T. Irifune, Y. Higo, T. Inoue, Y. Kono, H. Ohfuji, and K. Funakoshi, Sound velocities of majorite garnet and the composition of the mantle transition region, *Nature* **451**, 814 (2008).
- [40] R. C. Liebermann, Pressure and temperature dependence of the elastic properties of polycrystalline trevorite (NiFe_2O_4), *Phys. Earth Planet. Inter.* **6**, 360 (1972).
- [41] B. Li, Compressional and shear wave velocities of ringwoodite γ - Mg_2SiO_4 to 12 GPa, *Am. Miner.* **88**, 1312 (2003).
- [42] G. R. Rigby, G. B. H. Lovell, and A. T. Green, The reversible thermal expansion and other properties of some magnesian ferrous silicates, *Trans. Br. Ceram. Soc.* **45**, 237 (1946).
- [43] A. Roldan, D. Santos-Carballal, and N. H. de Leeuw, A comparative DFT study of the mechanical and electronic properties of greigite Fe_3S_4 and magnetite Fe_3O_4 , *J. Chem. Phys.* **138**, 204712 (2013).
- [44] (a) Y. Ishikawa and Y. Syono, Giant magnetostriction due to Jahn-Teller distortion in Fe_2TiO_4 , *Phys. Rev. Lett.* **26**, 1335 (1971); (b) Y. Syono, Y. Fukai, and Y. Ishikawa, Anomalous elastic properties of Fe_2TiO_4 , *J. Phys. Soc. Jpn.* **31**, 471 (1971).
- [45] S. M. Antao, I. Jackson, B. Li, J. Kung, J. Chen, I. Hassan, R. C. Liebermann, and J. B. Parise, High-temperature elasticity of magnesioferrite spinel, *Phys. Chem. Miner.* **34**, 345 (2007).
- [46] I. Jackson, S. K. Khanna, A. Revcolevschi, and J. Berthon, Elasticity, shear-mode softening and high-pressure polymorphism of wüstite (Fe_{1-x}O), *J. Geophys. Res.* **95**, 21671 (1990).
- [47] D. Isaak and S. Moser, Elasticity of single-crystal wüstite at ambient and elevated temperature from resonant ultrasound spectroscopy, *J. Phys. Chem. Solids* **74**, 879 (2013).